INFLUENCE OF HONEYCOMB RUBBING ON TIP SEAL PERFORMANCE OF TURBINE ROTOR

D. Frączek, W. Wróblewski, T. Chmielniak

Institute of Power Engineering and Turbomachinery,

Silesian University of Technology, Gliwice, Poland

ABSTRACT

The small radial gap of the rotor tip seal leads to the rubbing of a honeycomb in take-off conditions and the leakage flow increases in the cruise conditions. The aim of this study is to compare two honeycomb seal configurations of low pressure gas turbine rotor. In the first configuration the gap is small and a rubbing takes place. In the second the fins of the seal are shorter to eliminate the rubbing. The study of geometrical model of honeycomb was performed to reduce the computational effort. The problem was investigated numerically using RANS equations and the two-equation SST turbulence model. The full honeycomb structure was taken into consideration to show details of fluid flow. The main parameters in the gap and leakage flows were compared and discussed. The assessment of leakage flow through the seal variants could support a design process.

Nomenclature

A - seal clearance area ($l \cdot s_{mean}$)
C_D - discharge coefficient
l - domain width
$\dot{m}$ - mass flow rate
u,v,w - axial, radial, circumferential velocity
i,j,k - axial, radial, circumferential velocity versor components
y^+ - dimensionless wall distance
p - pressure
r - domain height
R - specific gas constant
s - seal clearance
U - velocity
Π - pressure ratio (p_{01}/p_{04})
ζ - geometrical parameter of the gap
κ - adiabatic exponent

Subscripts
0 - stagnation
1,3 - inlet
2,4 - outlet
eff - effective
nom - nominal

Introduction

A reduction in leakage flows in turbomachines and the machinery safe operation are two factors which need to be considered in a design process simultaneously. Aircraft engines operate under different loads which vary the mutual positioning of the rotating and stationary parts. Labyrinth seals with a honeycomb land are mostly used in these cases to prevent the seal failure and to weaken the effect of rubbing. Apart from the gap tolerance, an important advantage of honeycomb seals is their reliability under temperature changes.

The gas flow through the honeycomb seal is complex and determined by the rotor shroud, the fin seal cavities and the honeycomb shape. The gap between the fins of the rotor shroud and the honeycomb land in cruise conditions should be minimal. However, in take-off conditions, the gap gets smaller and rubbing can occur. As a result, the gap over the fin gets bigger in cruise conditions and leakage flow may increase. The honeycomb rubbing may reduce the efficiency of the turbine up to 1% Razak (2007). Before making a decision to avoid rubbing under transient loads, it is vital that the flow structure in the seal domains and the seal performance with and without rubbing should be assessed.

Many authors investigated flows through the seal channels both experimentally and numerically. Kim, et al., (2009) compared the CFD results and experimental data with analytical results for straight and stepped seals. They perform steady computations with realizable k-epsilon turbulence model using STAR-CCM+. The computation results coincide well with the experimental data and analytical formulae in the case of the straight seal. For the stepped seal, the CFD and experimental results deviate slightly from the analytical one. The authors suggested that the analytical model does not reflect exactly the stepped geometry of the seal.

Schramm, et al., (2002) analyzed the flow through the seal with and without a honeycomb land experimentally and numerically. The honeycomb facing provides an enlarged effective gap and results in an increased leakage mass flow rate. Compared to the smooth configuration, the dependence of the flow field on the gap was significantly reduced. The numerical results got similar to the LDV measurements.

Li Jun, et al., (2010) conducted a numerical analysis of the influence of the main parameters of the seal on the leakage volume. They used the commercial CFX code and solved the RANS equations with the standard k-ε turbulence model. They stated that the leakage flow rate grew as the sealing gap increased. The minimum leakage flow rate was reached when the honeycomb cell diameter was equal to the labyrinth step. They gave the optimal depth of the honeycomb and observed the increase in the leakage flow rate for higher rotational speed due to the increase intensity of recirculation inside the seal chamber.

Denecke, et al., (2003) analyzed the impact of the stator rub-grooves on the labyrinth leakage. Experimental and computational investigations showed a possibly large influence of rub-grooves on the seal performance. The analysis comprised three labyrinth seal types: seals covered straight-through, seals stepped with forward facing steps and seals stepped with backward facing steps. The authors determined the dependence of the leakage mass flow on fins and the geometry of rub-grooves. They found the seal geometrical features which can be used to assess the leakage characteristics. The leakage through the seal causes mixing losses and additionally affects the main flow stability in the subsequent stage. Biester, et al., (2011) analyzed the interaction of the leakage flow with the main flow. Time-resolved CFD simulations showed a strong non-uniformity of the leakage flow depending on the circumferential position of the up- and downstream blades. The re-entry of the leakage into the blade-to-blade domain results in the formation of a counter-rotating vortex. The leakage interaction with the main flow is limited to the end walls, with almost no influence on the mid-span flow. The authors compared steady state and time-resolved predictions. The steady state results displayed the secondary flow effects with limited accuracy.

Denecke, et al., (2005) carried out an experimental investigation of the total temperature increase due to internal losses (windage heating) and the swirl development in convergent and divergent stepped labyrinth seals. The change in the total temperature across the seal was sensitive to small local differences of the swirl velocities within the gap. A test rig with a rotating disc was used to measure the leakage flow parameters at different rotational speeds, for different pressure ratios and inlet swirls. They used a two-cell pitch honeycomb model and solved the 3D RANS equations using a realizable k-ε turbulence model. The results were in good agreement with experimental data.
The same simplification of the honeycomb land was used by Wróblewski, et al., (2010). The authors described the optimization of the fin seal shape, which resulted in a reduction in leakage by about 16%.. The analysis based on the Goal-Driven Optimization was conducted including all parameters used in the optimization process. In the Goal-Driven Optimization a set of ten geometrical parameters was taken into account.
The objective of the present study is to compare the two cases of the seal with a honeycomb land. The first configuration is the reference geometry and has rub-grooves over the fins made during the turbine transient operation. The geometry of the rub-grooves was defined based on inspection data. The second variant of the seal configuration has shorter fins to eliminate rubbing. Both these cases are analyzed in cruise conditions with an assumption that the nominal fin gaps are equal.

Model definition

Modelling the honeycomb land structure is challenging, mainly because of the large number of honeycomb cells which are small in relation to the main flow domain defined for the blade-to-blade channel. Biester, et al. (2011) showed that the leakage interaction with the main flow is limited to the end walls, with almost no influence on the mid-span flow. Therefore, the main flow domain of the blade-to-blade channel was reduced to the tip region comprising about 10% of the channel height. In the next step, the main flow domain was replaced with inlet and outlet chambers, where at the chamber boundaries parameters obtained from the main flow simulations were assumed. As a result, the honeycomb circumferential pitch instead of the blade cascade pitch now determines the periodicity of the computational domain. This kind of domain simplification was successfully used in Wróblewski, et al., (2010). . Computations were made taking into account a honeycomb land with and without rubbing. The seal geometries are presented in Fig. 1.
Boundary conditions were defined at inlets (Fig. 1b cross section 1 and 3) and at outlets (Fig. 1b cross section 2 and 4) of both main flow chambers. Locations of boundary conditions and their shape were simplified and shifted as well to avoid possible convergence problems. Dashed lines (Fig. 1b A1, A2, A3, A4) depict cross sections where the flow data were given while solid lines (1-4) define the fluid domain boundaries. A numerical analysis was performed for three-dimensional models of the seal flow domain with a pitch of two, four and six honeycomb cells.
The boundary layer on the honeycomb walls which separate every single cell should be modelled. The number of cells in the seal is huge and, in consequence, the number of the mesh elements would rise significantly. Therefore, boundary layers were only modelled in cells located directly above the fins. This allowed for a better simulation of flow phenomena in areas above fins with the highest velocity. Dimensionless wall distance y^+ was less than 2 for cells with ogrid and for honeycomb cells without ogrid y^+ was up to 14.
The commercial code ANSYS CFX 15 was used for numerical simulations. The ideal gas model was assumed. The Sutherland formula was used to take the temperature dependence of the viscosity coefficient into account. The flow was steady and adiabatic. For turbulence modelling, the two-equation k-ω SST turbulence model was chosen. The energy equation included the viscous work term. The higher order upwind advection scheme was selected to solve the governing equation system. Convergence criteria for residuals were set on RMS$<10^{-4}$.
Inlet boundaries of chambers (cross sections 1 and 3, Fig. 1b) the circumferentially averaged

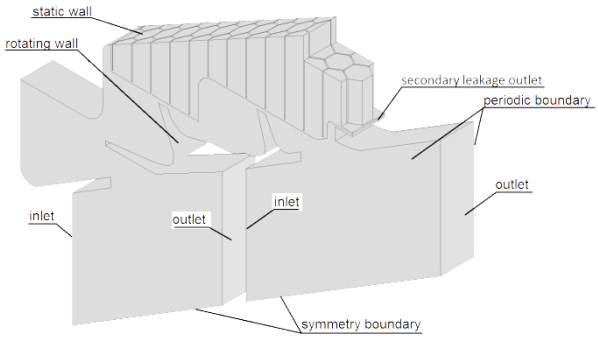

a) **domain boundaries**

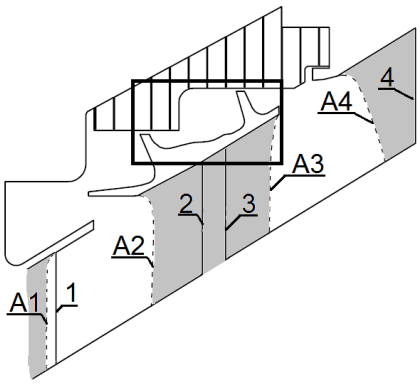

b) chambers inlets and outlets

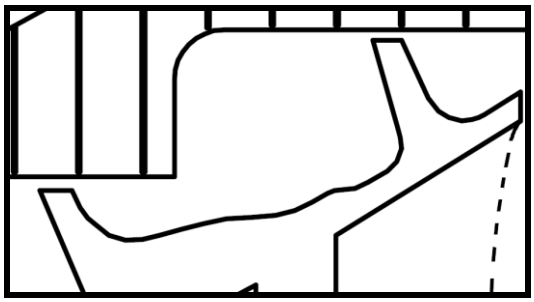

c) without rubbing

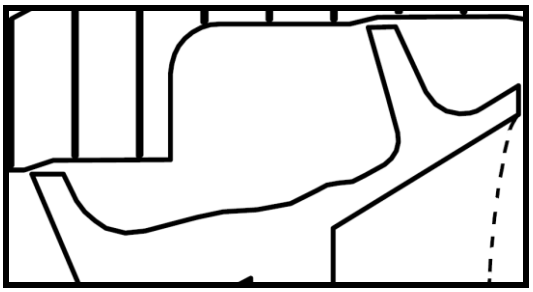

d) with rubbing

Fig. 1 Computational domain ((dashed lines - edges of the blades)

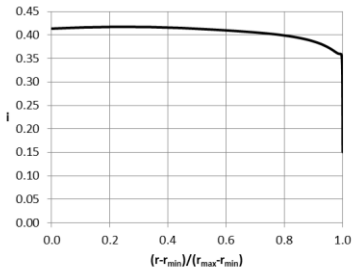

a) Axial component of velocity versor

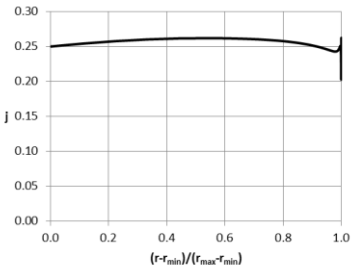

b) Radial component of velocity versor

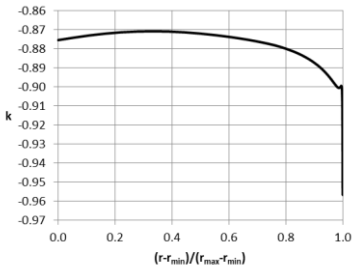

c) circumferential component of velocity versor

Fig. 2 Inlet A1 boundary condition

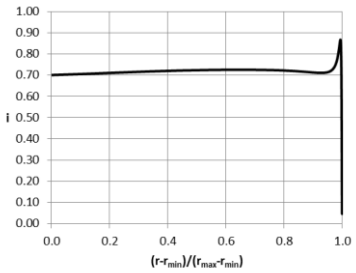

a) Axial component of velocity versor

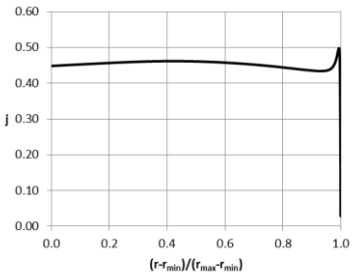

b) Radial component of velocity versor

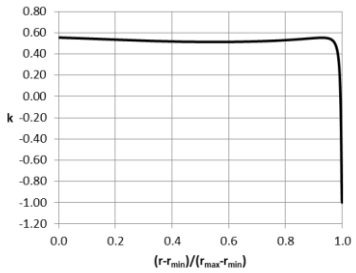

c) circumferential component of velocity versor

Fig. 3 Inlet A3 boundary condition

distributions of the velocity versor component (Fig. 2 and Fig. 3), the total pressure and the total temperature are defined based on the results of a multistage flow simulation. In addition, the mass flow rate for secondary leakage flow $\dot{m}_{out} = 10\ kg\ m^{-2}\ s^{-1}$ was assumed at the secondary leakage outlet (Fig.1a). The static pressure distributions at outlets (cross sections 2 and 4, Fig. 1b) were assumed. The pressure ratio for the simulation was 1.1. The bottom boundary was set close to the streamline and therefore the symmetry condition is assumed. The circumferential periodicity is defined and an adiabatic condition is selected for the remaining walls.

The mesh generation plays an essential role in the fluid flow modelling. The flow structure in the labyrinth seal with a honeycomb is three-dimensional and strongly influenced by the gas expansion, the high relative rotational speed and turbulence. In the flow field, strong gradients are present and high velocity as well as stagnation regions can be distinguished.

The numerical mesh in the chambers and in the labyrinth seal was built as a hexa-dominant surface mesh and then extruded along the circumferential direction. Separately in the honeycomb domain, a fully 3D structured, multiblock mesh was generated. In the honeycomb cells, directly above the fins, the boundary layer was discretized with a finer mesh compared to the other cells. The two grids: the honeycomb structured grid and the unstructured seal grid were merged. The position of the grid interface was selected approximately in a third of the gap span. This location is different from models typically used in numerical studies (e.g. Schramm, 2002), where the interface was defined exactly at the end of the honeycomb walls. Such location of the interface allows a proper discretization around the honeycomb walls. At the interface, the General Grid Interface option is used, which allows a proper connection of grids to non-fitting nodes.

The correct solution to the flow patterns should be mesh-independent. To check this property of the solution, a numerical study with seven different mesh sizes with 670k, 970k, 1.3M, 1.7M, 2.4M, 3.2M and 4.7M grid nodes were used for the mesh dependency test. It was performed for the case without rubbing. The initial mesh with 670k nodes was not refined globally, but in the regions with greater parameter gradients. Fig. 4 present the discharge coefficient C_D versus the number of nodes in the simulation. Discharge coefficient is defined as:

$$C_D = \frac{\dot{m}}{\dot{m}_{ideal}} \tag{1}$$

$$\dot{m}_{ideal} = \frac{p_{01} A}{\sqrt{T_0}} \sqrt{\frac{2\kappa}{R(\kappa - 1)} \left[\left(\frac{1}{\Pi}\right)^{2/\kappa} - \left(\frac{1}{\Pi}\right)^{(\kappa+1)/\kappa} \right]} \tag{2}$$

The mass flow $\dot{m}$ was defined as the difference between the mass flow passing the inlet boundary (cross section 1) and outlet boundary (cross section 2). The maximum difference in the mass flow rate was about 3.7%, and for meshes with more than 1.7M nodes, the deviation was less than 0.7%. This indicates that acceptable tolerance was reached, and the 1.7M-node mesh can be used for a further analysis. The final mesh is shown in Fig. 5. The mesh has the maximum value of y^+ less than 14, but in the regions close to the rotor walls – y^+<2.

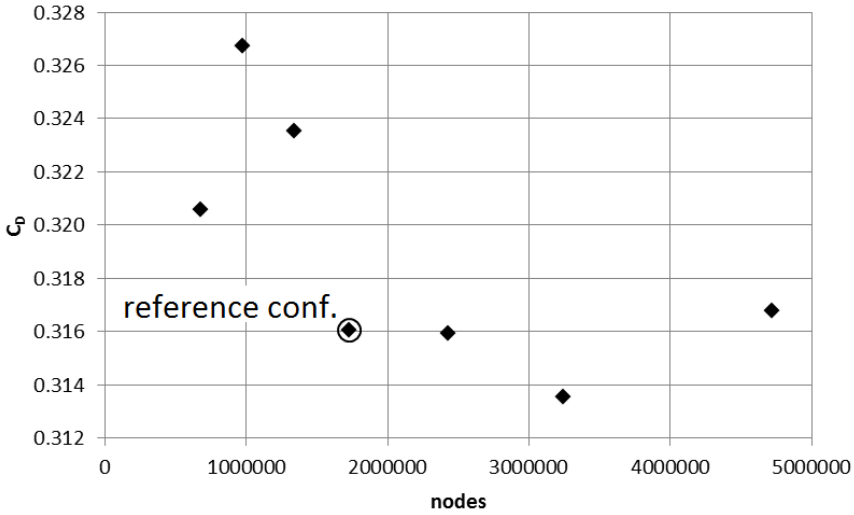

Fig. 4 Discharge coefficient vs the number of mesh nodes

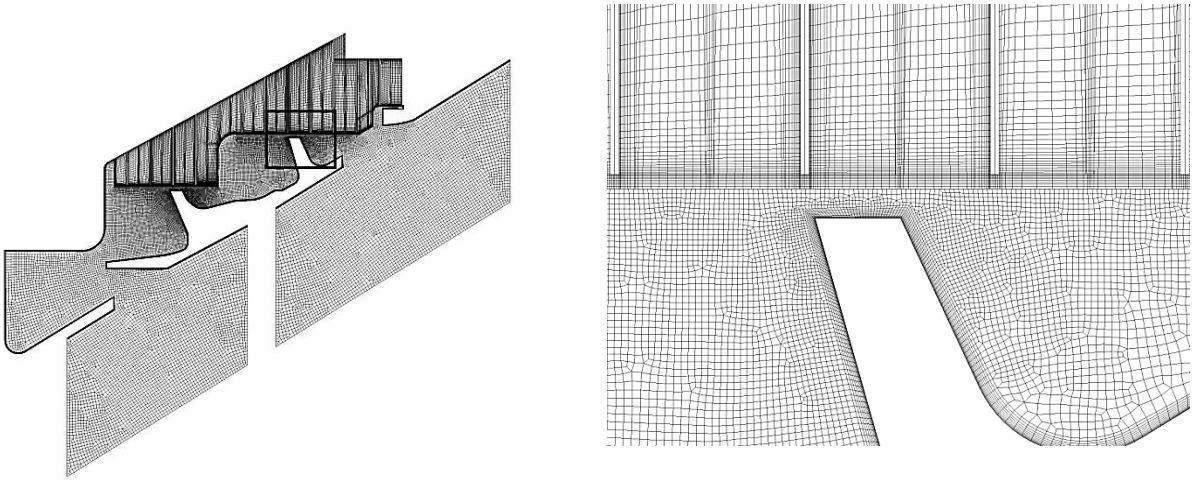

a) Entire mesh in the seal domain

b) Mesh in the region above the second fin

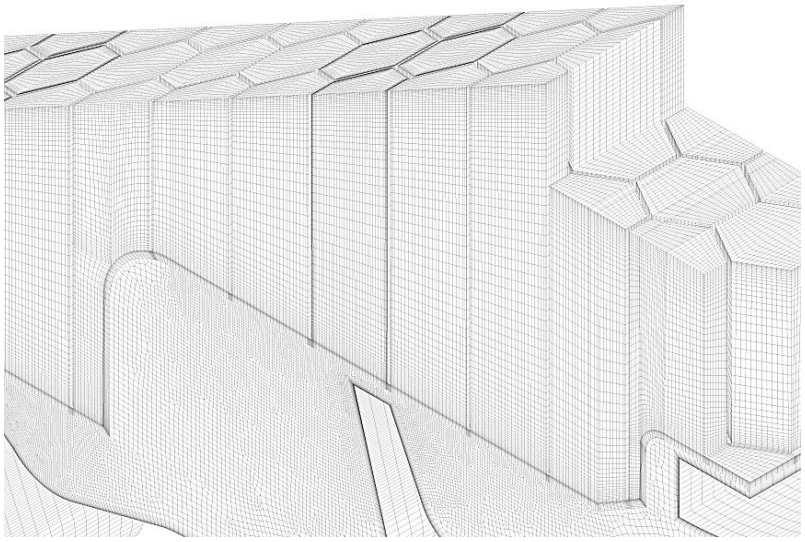

c) Isometric view of the mesh

Fig. 5 Overview of the computational mesh

Results

The two geometrical definitions of the honeycomb: with and without rubbing are very similar regarding the main parameters. The leakage flow is sensitive to a change in geometrical parameters, especially in the region located directly above the fins. If the gap of the seal with a honeycomb is small, it is necessary to define the effective gap and the effective surface area. According to Schramm, et al., (2002), the effective gap is found from the following formula:

$$s_{eff} = \sqrt{\left(\frac{L-b}{2}\right)^2 + s_{nom}^2} \tag{3}$$

where L is the honeycomb cell size, b is the thickness at the seal fin tip and s_{nom} is the nominal gap. The definition of geometrical parameters of the seal is presented in Fig 6. Based on s_{eff}, averaged gap s_{mean} and the averaged change in the cross-section area available for the leakage flow ζ_{geom} can be defined as:

$$\zeta_{geom} = \frac{s_{mean}}{s_{nom}} \tag{4}$$

The value of s_{mean} is calculated for a specific configuration of fins and honeycomb cells. In the seal without rubbing, the shortening of the fins results in a bigger thickness at the fin tip, which involves a change in the ζ_{geom} parameter. On the other hand, in the seal with rubbing, the honeycomb geometry changes. The geometrical characteristics of the seal geometries are presented in Table 1. The gap geometries are defined taking into account the inclination of the honeycomb surface. The definition of geometrical parameters is not in this case straightforward because the value of s_{mean}

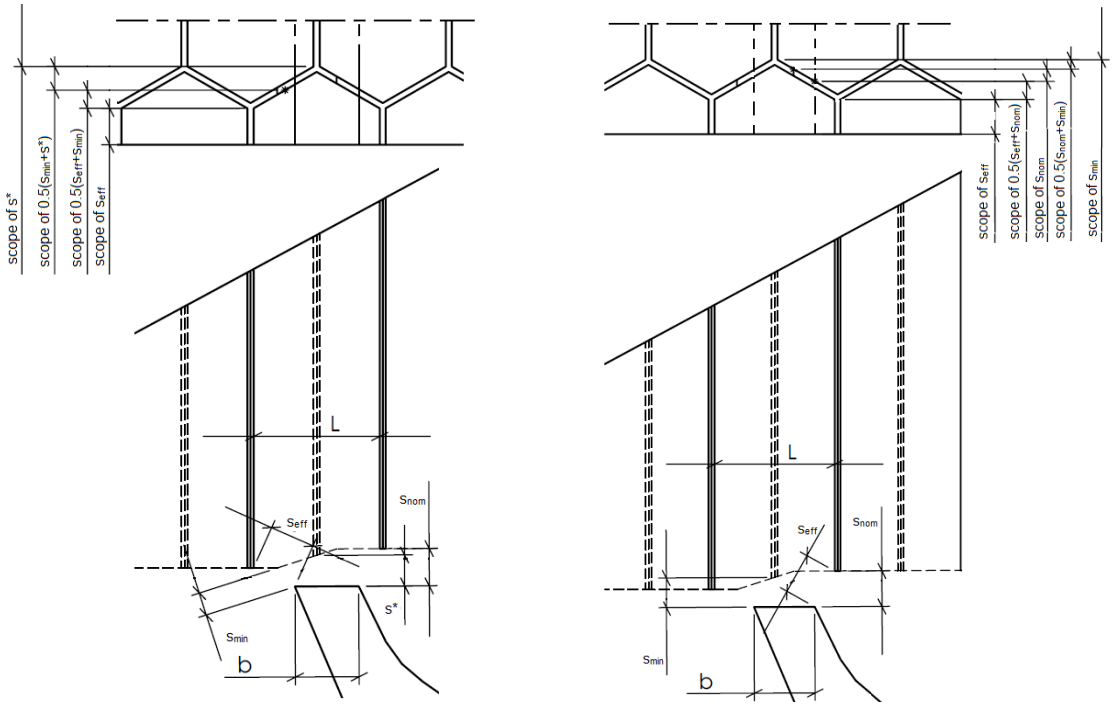

a) **Upstream fin edge** **b) Downstream fin edge**

Fig. 6 Definition of clearance parameters

Table 1 Comparison of geometrical parameters

First fin	s_{nom}	s_{mean} w/o rubbing	s_{mean} rubbing	ζ_{geom} w/o rubbing	ζ_{geom} rubbing
Upstream edge, *mm*	0.94	1.20	0.89	1.27	0.95
Downstream edge, *mm*	0.94	0.96	1.00	1.02	1.07

Second fin	s_{nom}	s_{mean} w/o rubbing	s_{mean} rubbing	ζ_{geom} w/o rubbing	ζ_{geom} rubbing
Upstream edge, *mm*	0.77	1.25	1.18	1.63	1.53
Downstream edge, *mm*	0.77	0.77	0.72	1.01	0.94

varies. For the first fin the value of s_{mean} for the upstream edge is much lower in the case with rubbing than in the case without rubbing. The location of the second fin in relation to honeycomb cells is very different than observed for the first fin (Fig. 6). The values of minimum s_{mean} calculated for the both fins decreases of 7%.

The numerical analysis of the flow in the labyrinth seal was conducted using different domain pitches to check the influence of the geometrical model on the solution. Meshes with three pitch values in the circumferential direction were made for the seal geometry, both with and without rubbing. The characteristics of the test cases are listed in Table 2. In case C1 (and in case C1r – with rubbing) two honeycomb cells in the circumferential direction were used, whereas in case C2 (C2r with rubbing) and C3 (C3r with rubbing) – four and six cells, respectively. The extension of the mesh was prepared by a geometric multiplication of the basic domain with the honeycomb two-cell pitch by factor 2 and 3.

The leakage mass flow rate reduction calculated according to the formula (5) for different pitches are: k_1=14.6%, k_2=15.2% and k_3=13.8%. The difference in results between the case C1 and other cases are less than 1pp and therefore the model of case C1 could be accepted for numerical simulations.

$$k_n = \frac{m_{Cn} - m_{Cnr}}{m_{Cn}} \tag{5}$$

where: n=1,2,3 is the case number.

The circumferentially averaged distributions of thermodynamic and kinematic parameters at cross section 4 are shown in Fig. 7. The results for all the test cases are very close to each other, regardless of the pitch or the presence of rub-grooves. The results are compared with the multistage flow simulation data to check correctness of the main flow approximation. . The calculated cylindrical velocity component along ¾ of the domain height has a shape similar to the reference data but it differs by about 10%. The axial and radial velocity components present a very similar tendency in the same height range but here the difference amounts to 5%. These small differences in axial velocity slope may contribute the difference in leakage mass flow between the case C1 and other cases. Slope for case C1 and slope for case C2 differs more than C1 than C1r which prevents

Table 2 Test cases for the domain pitch study

Case	Rubbing	Domain pitch
C1	no	2 hc cells
C2	no	4 hc cells
C3	no	6 hc cells
C1r	yes	2 hc cells
C2r	yes	4 hc cells
C3r	yes	6 hc cells

a simple relationship between velocity distribution at cross section A4 and seal leakage. The distribution of total pressure in Fig. 7d shows that in the region near the platform the calculated values are lower than the reference data, which is proved by higher losses. Summing up, all the calculated distributions deviate from the reference data over the range near the blade platform. In this region, the mixing of the leakage and the main flows takes place, which influences the parameter distributions. This phenomenon was not simulated in the whole turbine calculations from which the reference data were taken. The velocity averaged values are the same for all the cases under analysis Fig. 7. The mixing process and the mixing losses do not affect the flow through the seal but have an influence on the subsequent stage of the turbine. This problem is essential in terms of the stage performance but it was not considered in the seal flow analysis.

Case C1 and C1r were more accurately analysed. In Fig. 8 the velocity vectors and pressure contours are drawn showing the flow pattern inside the seal. The leakage jet accompanied by recirculation regions inside the seal cavities creates the main flow structure. The velocity vectors for variants C1 and C1r show that the main flow fields in both cases are very similar and only small differences in intensity and location of selected phenomena can be noticed. In the rubbed seal flow over the fin is more contracted. The 2D streamlines (Fig. 9) that passes the seal gap have more wavy shape. The leakage jet approaches the first fin gap axially. It flows round the large vortex appearing before the first fin. The situation at the inlet to the second fin is very different. The leakage jet flows round the vortex too but along its upper side, and then along the fin wall. The jet

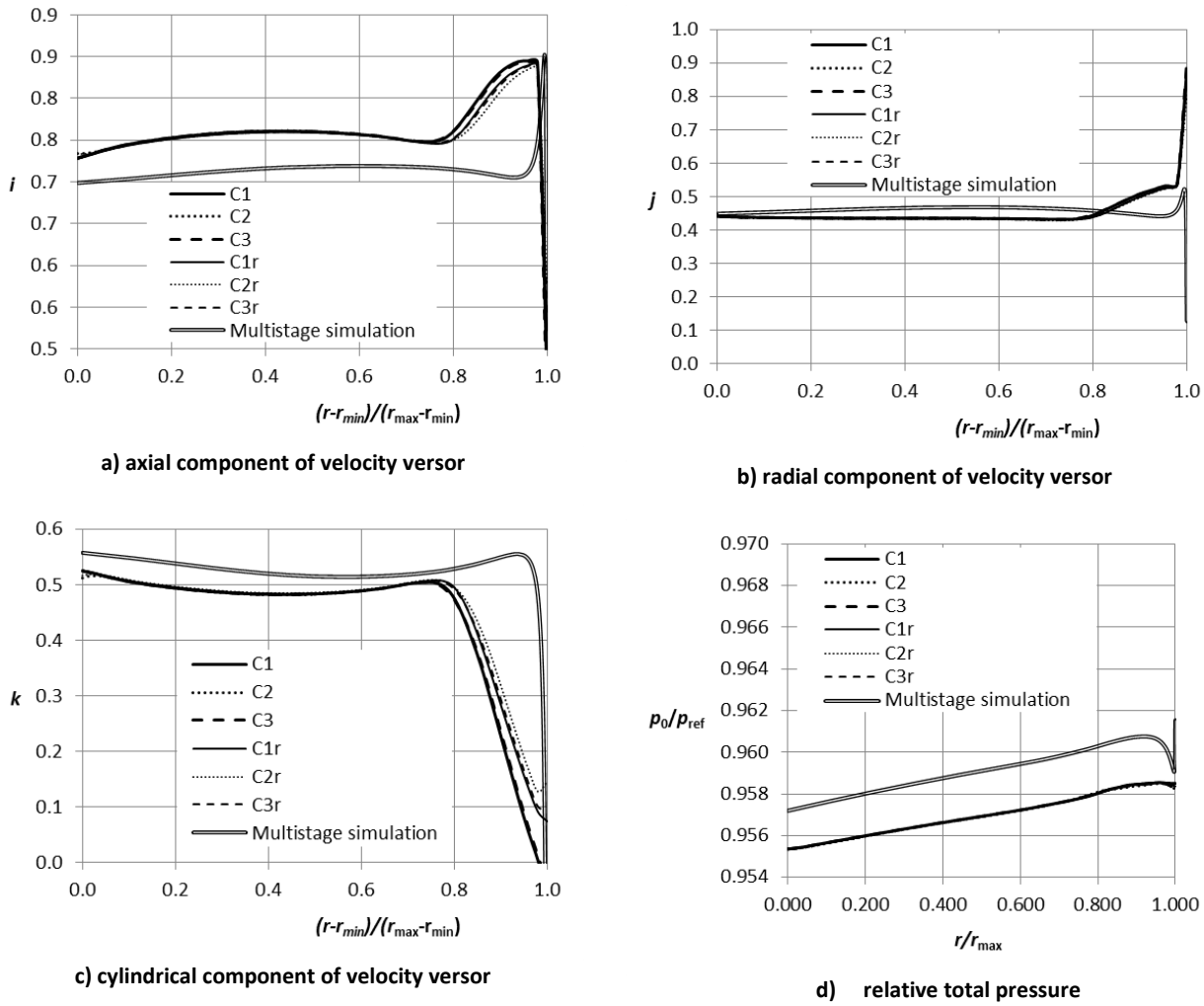

a) axial component of velocity versor

b) radial component of velocity versor

c) cylindrical component of velocity versor

d) relative total pressure

Fig. 7 Parameter distribution at cross section A4

reaches the fin gap radially. In this case, a contraction takes place at the fin tip. The structure of the flow inside the honeycomb cells is similar in both cases: without and with rubbing. Vortex structures are visible inside the honeycomb cells. A part of the leakage flow enters the honeycomb cells, where it creates a larger vortex. The analysis did not comprise the heat transfer to the honeycomb walls so these structures can only be attributed to dissipation of kinetic energy.
Fig. 10 presents the relative static pressure and relative velocity distributions along 2D streamlines presented in Fig. 8. The static pressure in the chamber between the fins is lower for the case C1r with rubbing than for the case C1. The flow resistances on the both fins are on the more similar level than for case C1 without rubbing. The maximum velocity for the case C1 is observed above the second fin. The velocities above the fins in the case C1r are almost the same.
In fig.11 the flow parameters distributions above the second fin including the honeycomb cell were presented. The velocities inside the honeycomb cell for the case C1 are about two times greater than for the case C1r at selected probe line. Inside the honeycomb cell the velocities have reached a level of 20% of the maximum velocity in the seal.

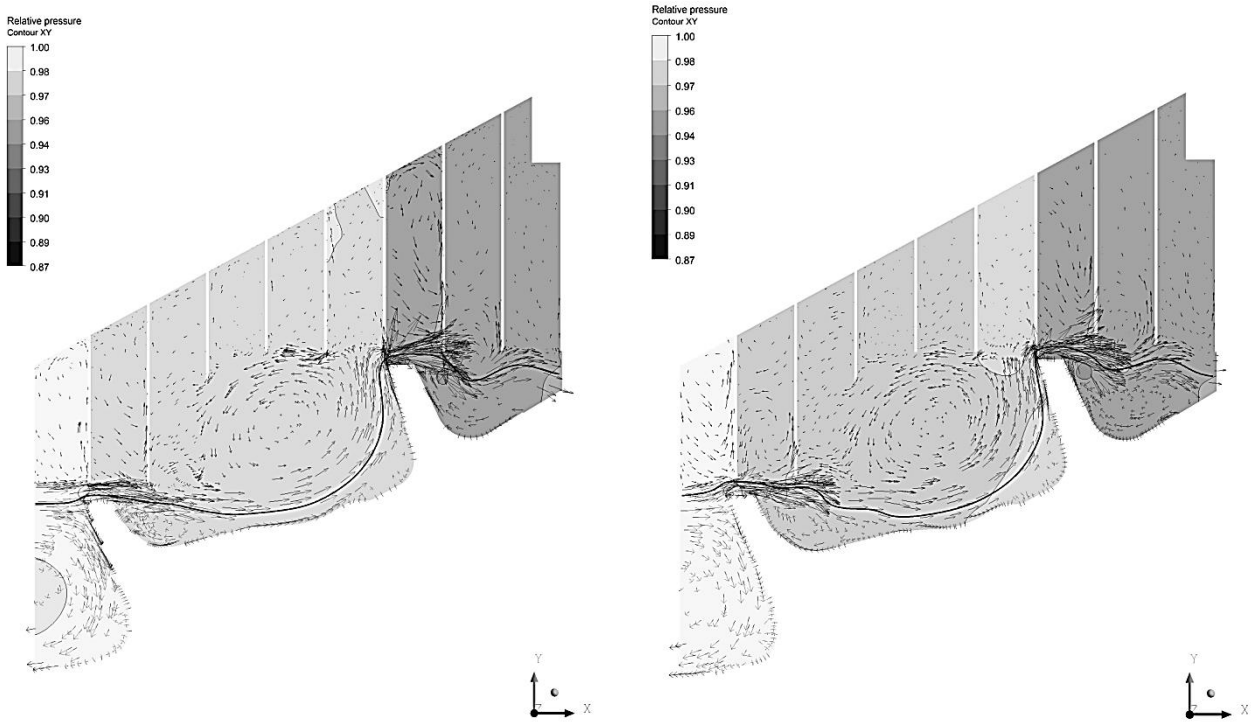

a) domain near the fins without rubbing **b) domain near the fins with rubbing**

Fig. 8 Velocity vectors and pressure contours on the XY plane

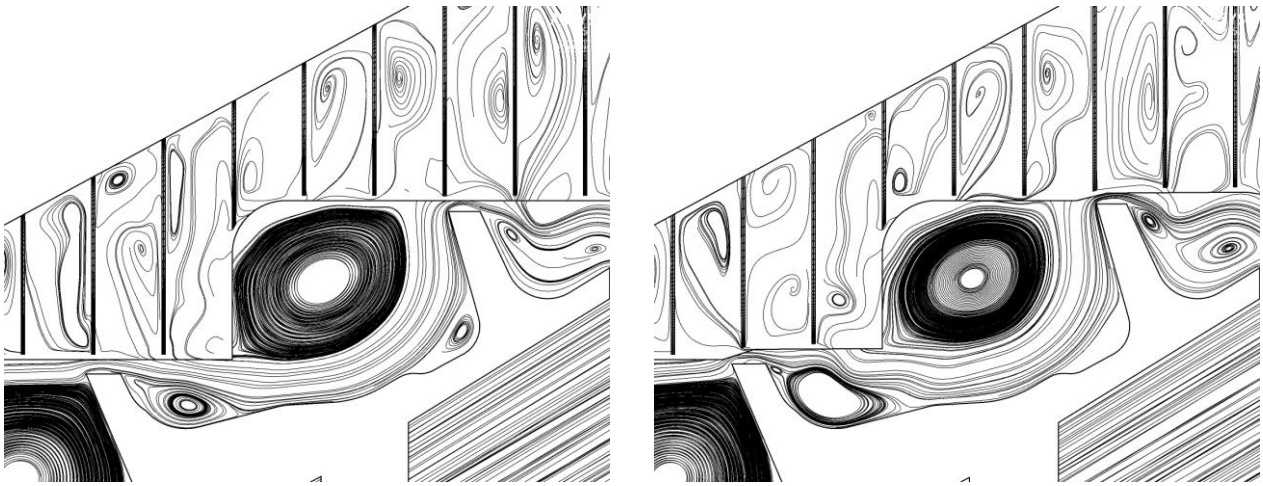

a) zoomed domain near the fins without rubbing b) zoomed domain near the fins with rubbing

Fig. 9 2D velocity streamlines on the XY plane

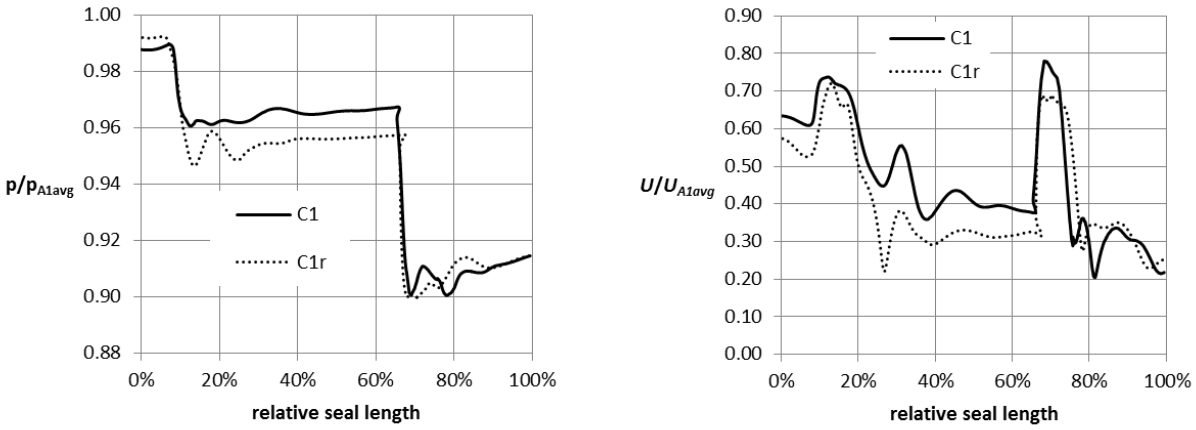

a) Relative static pressure b) Relative velocity

Fig. 10 Parameters along the leakage streamline

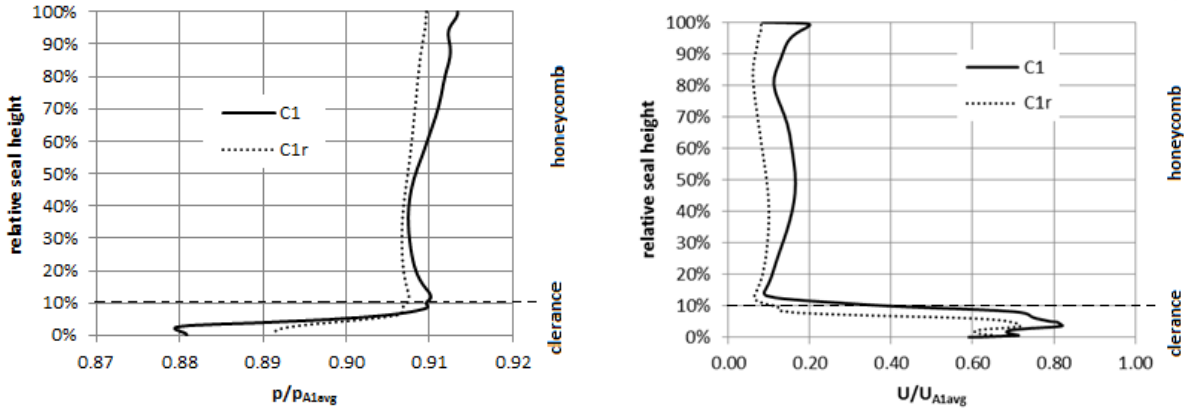

a) Relative static pressure b) Relative velocity

Fig. 11 Parameters above second fin

Conclusions

Numerical analyses of the rubbing effect on the labyrinth seal performance characteristics were carried out. Three-dimensional models of the labyrinth seal with the honeycomb land were proposed and tested. The real geometry of the turbine rotor seal was simplified to reduce the computational effort. The numerical models assumed the domain pitch of two, four or six honeycomb cells. The problem was investigated numerically using the RANS equations and the two-equation SST turbulence model. The honeycomb full structure was taken into consideration to show details of the fluid flow in the seal cavities and inside the honeycomb cells as well. The grid study shows that the use of the honeycomb model with a two-cell pitch is sufficient to simulate the global flow parameters properly. The labyrinth seal with honeycomb rubbing was compared to the honeycomb seal with shortened fins with regard to the flow structure and performance, and the comparison results were presented. The nominal gap is the same in both cases but the honeycomb surface over the fins has an inclination. It influences the performance of the seal. The values of minimum s_{mean} calculated for the both fins decreases of 7%. This reduction is lower than the mass flow rate reduction which was about 13%. The geometrical reduction has to be considered together with the flow field to assess the seal performance.
The presented model can be used to simulate the performance of labyrinth seals with a honeycomb land with satisfactory accuracy.

Acknowledgements

This work was supported by the National Centre for Research and Development and Avio Polska within the Innolot Programm, project Coopernik.

References

Biester, M.-O., Mueller, L., Seume, J. R., & Guendogdu, Y. (2011, June). GT2011-45883 Time-Resolved Numerical Investigation of the Interaction of Labyrinth Seal Leakage and Main-Flow in a 1.5-Stage LP Turbine. *Proceedings of the ASME Turbo Expo 2011, 5*, pp. 1623-1632.

Denecke, J., Dullenkopf, K., Wittig, S., & Bauer, H.-J. (2005, July). GT2005-68677 Experimental Investigation Of The Total Temperature Increase And Swirl Development In Rotating Labyrinth Seals. *Proceedings of ASME Turbo Expo 2005 -Power for Land, Sea, and Air, 3*, pp. 1161-1171.

Denecke, J., Schramm, V., Kim, S., & Wittig, S. (2003, April). Influence of Rub-Grooves on Labyrinth Seal Leakage. *Journal of Turbomachinery, 123*, pp. 387-393.

Kim, T. S., & Cha, K. S. (2009, October). Comparative analysis of the influence of labyrinth seal configuration on leakage behavior. *Journal of Mechanical Science and Technology, 23*, pp. 2830-2838.

Li, J., Kong, S., Yan, X., Obi, S., & Feng, Z. (2010, March). Numerical Investigations on Leakage Performance of the Rotating Labyrinth Honeycomb Seal. *Journal of Engineering for Gas Turbines and Power, 132*(062501).

Razak, A. (2007). *Industrial Gas Turbines - Performance and Operability.* Hardbound: Woodhead Publishing.

Schramm, V., Willenborg, K., Kim, S., & Wittig, S. (2002, January). Influence of a Honeycomb Facing on the Flow Through a Stepped Labyrinth Seal. *Journal of Engineering for Gas Turbines and Power, 124*, pp. 140-146.

Wróblewski, W., Dykas, S., Bochon, K., & Rulik, S. (2010, August). Optimization Of Tip Seal With Honeycomb Land In Lp Counter Rotating Gas Turbine Engine. *TASK Quarterly, 14*, pp. 189-207.